Vol. 26 • No. 30 • August 13 • 2014

D10488

www.advmat.de

ADVANCED MATERIALS

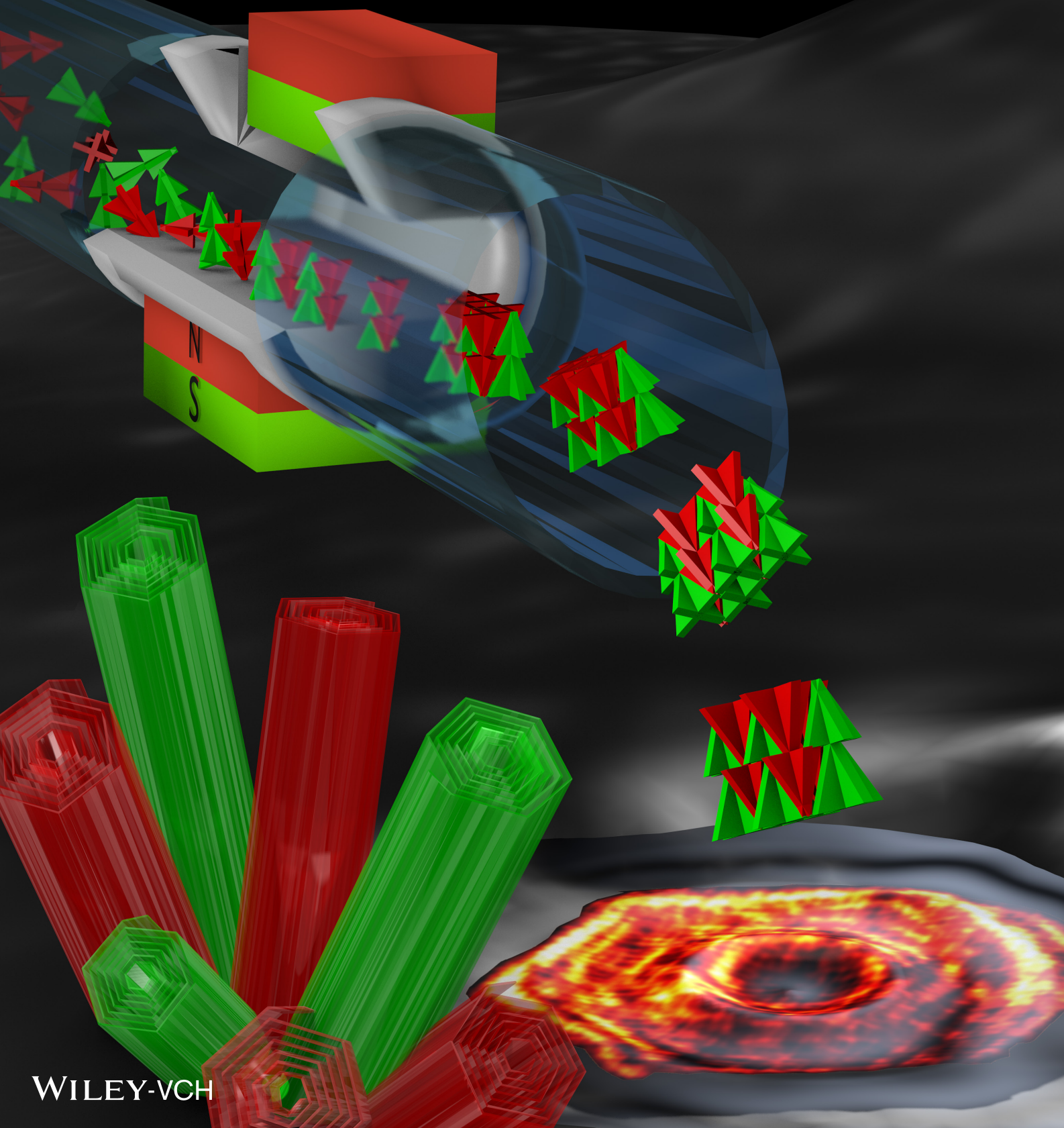

WILEY-VCH

Enhanced Self-Assembly of Metal Oxides and Metal-Organic Frameworks from Precursors with Magnetohydrodynamically Induced Long-Lived Collective Spin States

Eric Breynaert*, Jens Emmerich, Danilo Mustafa, Sneha R. Bajpe, Thomas Altantzis, Kristof Van Havenbergh, Francis Taulelle, Sara Bals, Gustaaf Van Tendeloo, Christine E.A. Kirschhock*, Johan A. Martens

Dr. E. Breynaert, Dr. J. Emmerich, Dr. D. Mustafa, Dr. S.R. Bajpe, Prof. F. Taulelle, Prof. C. E.A. Kirschhock, Prof. J. A. Martens
KULeuven – Center for Surface Chemistry and Catalysis. Kasteelpark Arenberg 23 – box 2461, B-3001 Heverlee, Belgium
E-mail: eric.breynaert@biw.kuleuven.be; christine.kirschhock@biw.kuleuven.be
T. Altantzis, K. Van Havenbergh, Prof. S. Bals, prof. G. Van Tendeloo
Electron Microscopy for Materials Science, University of Antwerp, B-2020 Antwerp, Belgium

Keywords: self-assembly, magneto-hydrodynamic synthesis, weak magnetic field, paramagnetic ions; electron spin coupling, long lived collective spin states

Low energy permanent magnetic fields (0.5T) applied in hydrodynamically turbulent conditions are observed to enhance self-assembly of geometrically frustrated spin systems (spin-glass, spin-ice or spin–liquid). This effect is demonstrated for the crystallization of vanadium oxide nano-scrolls, manganese oxide nano-tubes and HKUST-1 type $Cu_3(BTC)_2.3H_2O$ Metal-Organic Framework. Crystallization of these geometrically frustrated spin systems involves spin coupling and alignment of initially isolated paramagnetic metal ions, respectively V(IV), Mn(IV) and Cu(II) into molecular precursor units that self-assemble into the final material. The electromagnetic and hydrodynamic forces applied during magnetohydrodynamic precursor treatment induce a long lived state of collective spin order by the resonant coupling of magnetic field and turbulent structured flow. This altered magnetic alignment in the molecular precursor units consequently assist the self-assembly process. The presented experimental setup enables precise control over the magnetohydrodynamic conditions during synthesis, which will be essential to elucidating the detailed mechanism.

Molecular assembly involves the self-organization of pre-existing chemical units into larger, ordered structures.[1] While self-assembly can be driven merely by cooperative interaction

forces, dynamic phenomena and transient interactions or shapes play an important role in processes involving energy dissipation.[2,3] Literature provides examples of such energy dissipative self-assembly processes in a magnetic field. Grzybowski *et al.* demonstrated a dissipative self-assembling system generating high degrees of order from a disordered set of macroscopic paramagnetic discs floating at an air/water interface.[4] The rotation of an external magnetic field below the system forced the discs to self-organize into a hexagonal pattern of auto-rotating monomeric units as result of the competition between the magnetic and auto-rotation induced hydrodynamic forces. On a molecular scale, Coey *et al.* demonstrated how a permanent magnetic field (1T) can be used to create a self-contained tube of concentrated paramagnetic electrolyte solution flowing inside a solution of ultra-pure water.[5,6]

These examples demonstrate how the application of a static, external magnetic field on moving magnetic or electric dipoles (or vice versa) results in an accumulation of forces comprising the Lorenz force, field induced internal electric currents generating an opposing magnetic force and the hydrodynamic forces. In case of electrolyte solutions containing paramagnetic ions (charged magnetic dipoles) the resulting effective magnetic and electric fields are extremely complex, but still can be tuned to either suppress or augment convection and dispersion of paramagnetic ions in the solvent.[5]

The external forces acting on a flow of charged species can be controlled by guiding the flow through a restriction in a hydrodynamic (HD) system, with a permanent magnetic field perpendicular to the flow direction, the so-called magnetohydrodynamic (MHD) system.[6] MHD treatment with weak magnetic field has already been demonstrated to assist in formation of monodisperse emulsions,[7] in nano-aggregate breakup,[8,9] and in Mo-V-Sb mixed oxide catalyst synthesis.[10]

This manuscript reports on a new type of MHD induced phenomenon dramatically and permanently affecting self-organization and magnetic structure of spin-ice, spin-glass or

spin-liquid materials during wet-chemical synthesis. This effect is demonstrated by application of a weak permanent magnetic field (ca. 0.3 T) during synthesis of vanadium oxide nano-scrolls, manganese oxide nano-tubes and COK-16, a polyoxometalate encapsulating HKUST-1 type MOF in a magnetohydrodynamic device. The presented MHD system enables precise variation of the nonlinear flow-magnetic field dynamics by controlling the MHD parameters - flow and field.[11] Since the beneficial effects induced in the example materials are likely to occur in many systems, MHD synthesis of technologically advanced materials is expected to both represent significant economic value, and deepen the mechanistic understanding of dynamical self-assembly processes.[12,13]

Manganese oxide nanorods are rod-like morphologies of the 2x2 tunnel oxide hollandite, which are commonly synthesised by chemical reduction of dissolved permanganate followed by hydrothermal treatment.[14] In presence of K^+ cations, prolonged hydrothermal treatment converts the initially dense nanorods (diameter: 100 nm) into hollow nanotubes with a wall thickness of 30 nm via a chemical etching process.[15] Post-synthesis modifications changing the K^+ content in the 2x2 tunnel cavity allows tuning of the magnetic properties α-MnO_2 nanotubes by alteration of the distribution of Mn^{3+} and Mn^{4+} ions on the triangular lattice of the Kagomé oxide α-K_xMnO_2. Above x=0.1 the geometrical frustration of the spins leads to spin glass behaviour.[16]

Preparation of K^+ doped α-MnO_2 nanorods by hydrothermal treatment of a hydrodynamically mixed synthesis suspension (HCl + $KMnO_4$)[17] resulted in whorled, rodlike MnO_2 nanocrystals with poorly defined morphology and plenty of surface defects in the form of ongrown secondary crystallites. Addition of a weak permanent magnetic field (0.3 T) perpendicular to the flow in the HD device to create magnetohydrodynamic turbulent conditions, improved the self-assembly leading directly to nanotubes during hydrothermal treatment. As shown in **Figure 2 (**P-XRD and Electron Microscopy (EM)), the MHD pre-treatment induces the formation of well-defined hollow MnO_2 nanotubes, increases yield and

crystallinity, supresses formation of non-tubular crystals and surface-nucleation (XRD, Scanning EM, Transmission EM; see **Figures S4 – S5**). As shown by Luo *et al.*, the growth process of these hollow nanotubes involves initial self-assembly of dense nanorods, followed by chemical etching of the inner core. This process was shown to be higly dependent on the spin order in the structure,[15,16] and can be correlated with the dissolution of an antiferromagnetic inner core of α-MnO_2 (hollandite), in favour of an α-K_xMnO_2 (cryptomelane) shell with spin glass behaviour.[15,16,18] Therefore it can be hypothesized that the MHD turbulent conditions applied during pre-treatment induce a long lived state of collective spin order by the resonant coupling of magnetic field and turbulent structured flow (Couette type). The internal spin order of the nanoscopic building units consequently improves self-assembly and induces formation of perfectly aligned, hollow nanotubes, without any need for etching dense nanorods.

Vanadium oxide nanoscrolls can be synthesized from brightly yellow layered vanadium pentoxide. During the first stages of the synthesis, the layered V_2O_5 is intercalated with organic amine templates at room temperature.[19] During intercalation, diamagnetic V^{+5} is partially reduced to paramagnetic V^{+4}, a process accompanied with a progressive change in color from bright yellow via orange to deep brown-red, caused by a precursor with polarons that are mobile within the vanadium sheets. This precursor is best described as spin liquid system.[19,20] Upon hydrothermal treatment of this deep red precursor gel,[19] the mixed octahedral/tetrahedral layers flex to form vanadium nanoscrolls from alkylamine[VO_x] sheets, closely related to the structure observed in TMA[V_4O_{10}].[21] In a synthesis combining a stirred pre-treatment with the hydrothermal treatment non-uniform scrolls with low degrees of order of the scrolling are obtained. MHD treatment strongly enhances precursor formation resulting in deep red gels after 3 h of MHD treatment as compared to 6 h of pure HD treatment. Furthermore, MHD pre-treatment drastically improves intra- and inter-layer order, which upon hydrothermal treatment leads to unprecedented hexagonally scrolled materials (**Figure**

3). Commeinhes *et al.* demonstrated with polarized-light microscopy how application of a weak permanent field orients the nanoribbons comprising nematic vanadium pentoxide gels to form one single magnetic domain.[22] Translated to the MHD turbulent conditions prevailing during MHD pretreatment of the nanoscroll synthesis gel, the local formation of magnetic domains implies an alignment of the spins within and between neighbouring VO_x nanosheets during their presence in the magnetic field. This increase in correlation time can allow unpaired electron spins to evolve into weakly coupled electron spin structures.[23] The hexagonal scrolling can easily be rationalised considering the construction of the V_2O_5 sheets with chains of vanadium square pyramids (SP) with their apexes alternating up (U) and down (D) while sharing two neighbouring edges of the base. These UD chains share SP corners in such a way that they can be transformed to each other by a 120° rotation along a chiral 3-fold axis. Related structures are for example found in V_nO_{2n+1} hexagonal tunnel frameworks such as $Cs_{0.3}V_2O_5$ and $Cs_{0.35}V_3O_7$.[24]

In case of polyoxometalate encapsulated metal organic framework COK-16,[25,26] magneto hydrodynamic (MHD) synthesis results in the appearance of a double quantum excitation in the Electron Paramagnetic Resonance (EPR) spectrum (**Figure 1**) without changing the framework structure, according to X-ray Diffraction (XRD) (**Figure S 2**). These half-field transitions are typically observed when magnetic dipole/dipole coupling between Cu^{2+} sites or Cu^{2+} pairs gain importance, relative to the direct exchange or super-exchange coupling in the pairs. The rate limiting reaction steps in the synthesis of HKUST-1 type MOFs such as COK-16 is the conversion of isolated, paramagnetic Cu^{2+} ions into diamagnetic Cu_2^{4+} pairs in paddle wheels (**Figure 1**, inset left). Antiferromagnetic (AF) coupling between the Cu^{2+} spins in the paddle wheel occurs via a super-exchange mechanism. Comparison of the quantitative EPR spectra for COK-16 synthesized in presence and absence of magnetic fields (**Figure 1**) indicates significant differences in the magnetic ordering of the AF coupled paddle wheels. The lower intensity of the broad, isotropic Lorentzian component indicates improved long-

range antiferromagnetic ordering. Together with the appearance of a half-field transition in the powder EPR spectrum a significant, positive influence of the magnetic field on the formation of the EPR silent spin coupled copper dimers is evident. As expected both phases (MHD and HD only) contain a spectral component due to the presence of mononuclear, extraframework Cu^{+2} compensating the charge of the HPA units enclosed in the pores.[25] The broad, isotropic signal resulting from the inter-dimer interaction between the AF coupled [Cu-Cu]$^{4+}$ dimers, indicates increased diamagnetism of the phase crystallized in presence of the magnetic field. Because the structure does not change (as confirmed by XRD, Figure S 2), enhanced magnetic ordering between the paddle wheels can be concluded. Even without MHD mixing, the interaction between Cu^{2+} and Keggin ion induces dimerization of Cu^{2+} improving the formation of $Cu_3(BTC)_2.3H_2O$, allowing room temperature formation as opposed to the typical hydrothermal synthesis of HKUST-1.[26] This effect is clearly enhanced by the presence of the magnetic field, during the MHD synthesis. The half-field resonance in the EPR spectra of the MHD synthesized sample results from a formally forbidden double quantum coherence in a thermally populated triplet state. The magnetic treatment during self-assembly of the material clearly affects the efficiency of this coherence transfer. A similar half-field transition was observed by Veber *et al.* studying a temperature induced phase spin transition inducing a diamagnetic dilution of Cu(hfac)2LMe.[27] It should be noted that the 111 planes in the $Cu_3(BTC)_2.3H_2O$ structure resemble a Kagomé lattice with AF coupled Cu^{2+} pairs located on the corners of each triangle (Figure 1, inset right). Since Kagomé lattices count among the geometrically most frustrated magnetic systems,[28] the strong effect of relatively small magnetic fields becomes less surprising.

Magnetic field effects (MFEs) have been reported on chemical reactions with unpaired, spin correlated bi-radicals. MFEs can occur whenever radical pairs structurally or kinetically

evolve differently, depending on their spin state (Singlet, $|S_0\rangle$ or Triplet, $|T_0\rangle$,$|T_{-1}\rangle$,$|T_{+1}\rangle$).[*,29–31] This is mostly studied in the field of Chemically Induced Nuclear or Electron Polarisation spectroscopy (CIDNP and CIDEP), or solid state NMR DNP[30] using bi-radicals in situ prepared via homolytic decomposition of C-C bonds or stable bi-radicals specifically designed for DNP.[32] Initially, these radicals are strongly correlated and the exchange interaction locks the Larmor frequencies of their spins hence maintaining the energy difference between the singlet and triplet states. Following their creation, the radicals begin to diffuse apart, weakening the coupling and resulting in a weakly coupled electron (radical) pair just before complete separation. In this weak coupling regime, S-T transitions can be induced by several magnetic interactions: Δg mechanism (Zeeman coupling), hyperfine coupling, spin orbit coupling and their related relaxation processes (spin-spin, spin lattice).[33–35] Strength of these couplings and their effect on the rate of T-T interconversion and S-T intersystem crossing (ISC) depends on the chemical system, the inter-radical distance and external magnetic fields. For weakly coupled electron pairs in magnetic fields with strengths in the same order of magnitude as the nuclear hyperfine coupling energy (<1000 G), the hyperfine coupling mechanism can induce spin flips by spin exchange between an electronic and a nuclear spin ("double quanta"), hence conserving the total spin angular momentum. In higher fields, where the Zeeman splitting matches the S-T splitting due to exchange, either the $|T_{-1}\rangle$ or $|T_{+1}\rangle$ state becomes degenerate with $|S_0\rangle$ (for electron pairs with triplet or singlet ground states respectively) hence re-enabling the hyper-fine induced ISC. In addition, spin polarization in weakly coupled triplet-doublet pairs in external magnetic fields can also be expected to occur via energy transfer from a quartet or doublet precursor state.[23]

In contrast with the score of studies investigating MFEs in systems with geminal singlet or triplet-born spin correlated radical pairs [29,33,36–38] (e.g. created using laser flash photolysis),

[*] $|S_0\rangle = 1/\sqrt{2}(|\alpha\beta\rangle - |\beta\alpha\rangle)$; $|T_{+1}\rangle\ |\alpha\alpha\rangle$; $|T_0\rangle = 1/\sqrt{2}(|\alpha\beta\rangle + |\beta\alpha\rangle)$; $|T_{-1}\rangle\ |\beta\beta\rangle$

almost no research has been performed on MFE's involving initially uncorrelated radicals, e.g. dissolved paramagnetic metal ions or radicals.[39,40] Because ISC is typically much longer lived than diffusional migration of free radicals, such MFEs most often have been observed in micelle systems or systems with increased viscosity where cage reactions increase the lifetime of spin correlated radical pairs.[35,41]

Lifetimes of interacting spin systems are significantly increased when consisting of uni-molecular bi-radicals, micelles or in viscous solvents while spin polarization occurs via fast reactions. The MFEs described in this manuscript all occur in systems with initially uncorrelated paramagnetic ions forming AF coupled spin pairs during synthesis. Consideration of collisional spin pairing statistics readily indicates the importance of S-T ISC during formation of such spin coupled dimers with singlet ground states.[42,43] Since all examples describe solids formed during the MHD treatment, diffusion is expected to be limited, at least on local scale.

The lifetime of spin pairs adsorbed on the surface of the solid phase is probably sufficient to allow ISC, as demonstrated by NMR signal amplification by reversible exchange (NMR-SABRE), where reversible sorption of para-hydrogen in low magnetic field enables the transfer of spin polarization to a substrate which becomes hyperpolarized without chemical modification.[44] Furthermore, a surface can generate local magnetic field gradients, demonstrated to be beneficial for ISC enhancement.[45–47]

The present observations have some similarity with relatively weak magnetic fields also influence the ratio between the $CaCO_3$ allotropes calcite and aragonite.[48–51] Weak magnetic fields are also exploited to improve the quality of silicon and germanium single crystals grown by the Czochralski process.[52] Funasako *et al.* demonstrated how a weak external magnetic field (< 1T), applied during room temperature crystallisation of a paramagnetic ionic liquid induced long range magnetic order in the obtained ferrocenium.[53] While

experimental evidence for a strong effect of magnetic fields on self-assembly under hydrodynamic conditions is accumulating, the theoretical framework remains intangible.[54,55] The most comprehensive experimental realisations of long lived hyperpolarized spin states of weak magnetic order can be recognized in the interacting pairs of AF coupled spins in the $[Cu\text{-}Cu]^{4+}$ paddle wheel dimers found in MHD synthesized COK-16, or in the singlet long lived state of a pair of coupled spins ½ in magnetic resonance hyperpolarization. Though the long lived singlet states observed and experimentally used in NMR are within reach of theoretical treatment of pair of spins residing in collective spin assemblies, theoretical methodologies have not yet been implemented to allow full treatment within current computability limits. A new paradigm for coarser grain computational algorithms must become available before theoretical treatment in large-scale chemical systems could be achieved.

In contrast with the current limitations of theoretical treatment, the role of turbulent flow and magnetic field are confirmed to be related to field orientation, perpendicular to the flow, the flow speed, and the time of exposure to the magnetic field, with an additional internal fluctuation time determined by the weak inter-spin couplings. These four parameters not only control suppression of convection and decreased self-diffusion, resulting in an increase of residence time in collectively migrating density fluctuations, but also determine the timescale and frequency of exposure to the external magnetic field.

The simplicity of the presented experimental MHD device and the resulting control over the critical parameters, flow, magnetic field and total residence time in the magnetic field allows systematic experimental exploration of many systems within rigorously controlled physico-chemical conditions. Extension of the current device with frequency controlled alternating magnetic fields will also enable exploration of weak inter-spin coupling by tuning the devices resonant mode to the fluctuating internal inter-spin fluctuations.

Conclusions

This report describes how magnetically enhanced hydrodynamic synthesis significantly improves self-assembly and crystallisation of technologically and economically relevant materials containing interacting spin coupled paramagnetic metal ions. Asides increasing efficiency of the synthesis, the magnetic field permanently and drastically improves magnetic order in the material. The simplicity and versatility of the MHD strategy already enables its application for innovation of material synthesis processes and identification of materials potentially hosting long lived polarised spin states.

Similar to simple crystallisation, self-assembly in dynamic systems remains almost *terra incognita* because of the difficulty to measure and assess proper phenomena governing the transition from density fluctuation to crystallization. The presented magneto hydrodynamic (MHD) strategy enables the development of a new class of devices providing control over parameters that were considered out of reach of manipulation: suppression of self-diffusion, time length of coherent collective behaviour, time window of induction spin order. Nucleation, crystallization and morphological control are therefore accessible with a much broader range of physico-chemical controls for elucidating complex many-body spin systems that resisted advanced investigation up to now.

Although a general framework explaining the generation of long lived spin states and their impact during magnetically enhanced material synthesis is developing very fast, further improvements will be dependent upon experimental categorization of the score of physicochemical parameters potentially affecting this process needs to be simplified by experimental categorization derived from by systematic observations for different chemical systems. The development of inter-spin coupling of pairs in the different schemes of hyperpolarization in NMR can impact deeply the description of these long lived magnetic, albeit at a cost of developing a new generation of theoretical models for description of multi-spin magnetic interactions. As a result the presented results can be expected to stimulate

the exploitation of the magnetic field effects on material synthesis, and also to induce further developments in spectroscopies exploiting spin polarization.

Experimental Section

HKUST-1 type MOF COK-16 was prepared by dissolution of Cu(NO3)2.3H2O (Fluka) in a 10^{-3} M $H_3PW_{12}O_{40}$ (Fluka) solution prepared using a 50% vol. ethanol (VWR)-water solution containing 0.1 M $NaNO_3$. Upon complete dissolution, a 1.259 x 10^{-2} M 1,3,5-H_3Btc (Acros organics) solution prepared 50% vol. ethanol-water containing 0.1 M $NaNO_3$ in was added. After mixing the pH of all synthesis solutions was 3±0.1. 50 ml of the synthesis mixture was transferred to a transparent tube (Masterflex High Perfomance Tygon® 70 Lab tubing R-3603, with 8 mm inner diameter and total volume of 50 ml) equipped with a magneto hydrodynamic device and pumped at RT in a peristaltic pump (Cole Parmer High Performance Pump - Model I/P 77600-62) applying a flow rate of 4 L/min respectively in absence and presence of an external magnetic field (NdFeB block magnets, B = 0.3 T) oriented orthogonally to the flow direction.

Manganese oxide nanotubes were prepared in the MHD system describe above, using a synthesis recipe described in literature.[17] 0.39 g potassium permanganate ($KMnO_4$) was mixed with 0.82 mL hydrochloric acid (37 %) in 45 mL dest. water. The resulting mixture was aged for 10 minutes in the MHD system at a flow rate of 4 L/min, respectively in absence and presence of the external magnetic field. The final products were obtained after hydrothermal treatment at 140 °C for 12 h, dried in a vacuum oven overnight (40 °C) and analyzed by XRD, SEM and TEM.

Vanadium oxide nanoscroll synthesis was done by mixing 42 mL solvent (EtOH/H_2O = ½ vol/vol), 6.68 g of V_2O_5 (36.73 mmole) and 4.92 g of dodecylamine (26.54 mmole), corresponding to a surfactant-to-vanadium ratio of 0.36. The mixture (total volume: 50 mL) was filled in the tubing of the MHD system and aged for 6 h at 4 L/min respectively in

absence and presence of the external magnetic field oriented orthogonally to the flow direction. The resulting gel was transferred into a Teflon-lined autoclave (23 mL volume) and hydrothermally treated for 3 days. The as-synthesized nanotubes were filtered, washed with EtOH and hexane and also dried under vacuum.

Powder XRD patterns were obtained for all samples from 3 to 90 degrees 2θ using a Stadi P ($CuK_{\alpha 1}$, STOE & Cie GmbH) in θ-2θ geometry and capillary mode. STOE Software WinXPOW was used to process the data.

EPR spectra were measured on samples diluted in K_2SO_4 (4%wt) using a Bruker ESP 300E X-band EPR spectrometer at 295 K and 140 K, using 50 KHz magnetic field modulation and a microwave frequency of 9.594 GHz. The magnetic field was centered at 3415 G using a sweep width of 6000 G, the microwave power was set at 20 mW, the modulation amplitude at 4.48 G, the time constant and conversion time at respectively 10.24 and 40.96 ms, and the receiver gain at 1.25×10^4. The graphs were plotted using Igor Pro 6.2.

Tilt series for electron tomography were obtained using a FEI Tecnai G2 electron microscope, operated at 200 kV and equipped with a Fischione tilt-rotation model 2040 tomography holder. The high angle annular dark field-scanning transmission electron microscopy (HAADF-STEM) images were acquired from -70° to +72° using 2° tilt increments for each sample. Alignment and reconstruction of the series were carried out using the FEI Inspect3D software. The 3 dimensional reconstruction was based on the Simultaneous Iterative Reconstruction Technique (SIRT), as implemented in Inspect 3D software.

Supporting Information

Supporting Information is available online or from the author.

Acknowledgements

J. Maes, S. Use´ and W. Wouters are gratefully acknowledged for their continuous technical assistance. J.E and E.B. wish to acknowledge fruitful discussions with J. Vanacken. S.R.B thanks Dr. Arunakumar for initial discussions. We are grateful to Amudhakumari for constant help with literature. M. Seo and N. de Greef are kindly acknowledged for their assistance with initial TEM measurements on the manganese and vanadium oxide nanotubes, E. Gobechiya for assistance with PXRD measurements.

Author Contributions - E.B. designed the research plan, performed EPR characterisation and prepared the manuscript. J.E. contributed to the experimental design, synthesis and characterization of V/Mn nanotubes. D.M. and S.R.B worked on COK-16 synthesis. T.A and K.V.H. performed the TEM/tomography activities coordinated by S.B. and G.V.T. F.T and C.E.A.K contributed to the structural characterisation and to the interpretation of the results. J.A.M initiated and supported weak magnetic field assisted synthesis research. All authors assisted in the writing of the publication and have given approval to the final version of the manuscript.

Funding Sources - We thank the Flemish Government for long-term structural funding (Methusalem). E.B. acknowledges the Flemish FWO for a postdoctoral fellowship. J.E. acknowledges financial support by the "Institute for the Promotion of Innovation through Science and Technology in Flanders (IWT-Vlaanderen)". G. V.T. acknowledges funding from the European Research Council (ERC grant nr. 24691 - COUNTATOMS). G. V. T. and S. B. appreciate financial support from the Integrated Infrastructure Initiative N. 262348 European Soft Matter Infrastructure, ESMI and European Union FP7 program -Marie Curie (IEF) respectively. The Flemish government is acknowledged for long-term structural funding (Methusalem) and the Belgian government for financing interuniversity poles of attraction (IAP-PAI). FT thanks KULeuven BOF for and SF fellowship.

[1] A. F. Demirörs, P. P. Pillai, B. Kowalczyk, B. a Grzybowski, *Nature* **2013**, *503*, 99–103.

[2] A. Bricard, J.-B. Caussin, N. Desreumaux, O. Dauchot, D. Bartolo, *Nature* **2013**, *503*, 95–98.

[3] G. M. Whitesides, B. Grzybowski, *Science* **2002**, *295*, 2418–21.

[4] B. Grzybowski, H. Stone, G. Whitesides, *Nature* **2000**, *405*, 1033–6.

[5] J. M. D. Coey, R. Aogaki, F. Byrne, P. Stamenov, *Proc. Natl. Acad. Sci. U. S. A.* **2009**, *106*, 8811–8817.

[6] M. S. Tillack, N. B. Morley, in *Stand. Handb. Electr. Eng.* (Eds.: D.G. Fink, H.W. Beaty), McGraw-Hill, New York, **1998**, p. 88.

[7] S. Kerkhofs, H. Lipkens, F. Velghe, P. Verlooy, J. A. Martens, *J. Food Eng.* **2011**, *106*, 35–39.

[8] B. Stuyven, G. Vanbutsele, J. Nuyens, J. Vermant, J. A. Martens, *Chem. Eng. Sci.* **2009**, *64*, 1904–1906.

[9] B. Stuyven, Q. Chen, W. Van De Moortel, H. Lipkens, B. Caerts, A. Aerts, L. Giebeler, B. Van Eerdenbrugh, P. Augustijns, G. Van Den Mooter, J. Van Humbeeck, J. Vanacken, V. V Moshchalkov, J. Vermant, J. A. Martens, *Chem. Commun.* **2009**, *0*, 47–49.

[10] B. Stuyven, J. Emmerich, P. Eloy, J. Van Humbeeck, C. E. A. Kirschhock, P. A. Jacobs, J. A. Martens, E. Breynaert, *Appl. Catal. A Gen.* **2013**, DOI:10.1016/j.apcata.2013.07.039, In Press, Correc.

[11] J. C. Richard, *J. Comput. Nonlinear Dyn.* **2013**, *8*, 031010.

[12] G. Ertl, *Science* **1991**, *254*, 1750–5.

[13] G. Ertl, *Angew. Chem. Int. Ed. Engl.* **2008**, *47*, 3524–35.

[14] Y. Muraoka, H. Chiba, T. Atou, M. Kikuchi, K. Hiraga, Y. Syono, S. Sugiyama, S. Yamamoto, J.-C. Grenier, *J. Solid State Chem.* **1999**, *144*, 136–142.

[15] J. Luo, H. T. Zhu, H. M. Fan, J. K. Liang, H. L. Shi, G. H. Rao, J. B. Li, Z. M. Du, Z. X. Shen, *J. Phys. Chem. C* **2008**, *112*, 12594–12598.

[16] J. Luo, H. T. Zhu, J. K. Liang, G. H. Rao, J. B. Li, Z. M. Du, *J. Phys. Chem. C* **2010**, *114*, 8782–8786.

[17] W. Xiao, H. Xia, J. Y. H. Fuh, L. Lu, *J. Power Sources* **2009**, *193*, 935–938.

[18] R. Zeng, J. Q. Wang, W. X. Li, G. D. Du, Z. X. Chen, S. Li, S. X. Dou, **2012**.

[19] J. Emmerich, E. Breynaert, C. E. A. Kirschhock, J. A. Martens, *Catal. Today* **2012**, *192*, 63–66.

[20] H. Kweon, K. W. Lee, C. E. Lee, *J. Appl. Phys.* **2010**, *108*, 023905.

[21] J. Livage, *Materials (Basel).* **2010**, *3*, 4175–4195.

[22] X. Commeinhes, P. Davidson, C. Bourgaux, J. Livage, *Adv. Mater.* **1997**, *9*, 900–903.

[23] A. van der Est, M. Asano-Someda, P. Ragogna, Y. Kaizu, *J. Phys. Chem. A* **2002**, *106*, 8531–8542.

[24] P. Y. Zavalij, M. S. Whittingham, *Acta Crystallogr. Sect. B Struct. Sci.* **1999**, *55*, 627–663.

[25] S. R. Bajpe, E. Breynaert, A. Martin-Calvo, D. Mustafa, S. Calero, C. E. A. Kirschhock, J. A. Martens, *Chempluschem* **2013**, *78*, 402–406.

[26] S. R. Bajpe, E. Breynaert, D. Mustafa, M. Jobbágy, A. Maes, J. A. Martens, C. E. a. Kirschhock, *J. Mater. Chem.* **2011**, *21*, 9768.

[27] S. L. Veber, M. V Fedin, K. Y. Maryunina, G. V Romanenko, R. Z. Sagdeev, E. G. Bagryanskaya, V. I. Ovcharenko, *Inorganica Chim. Acta* **2008**, *361*, 4148–4152.

[28] J. L. Atwood, *Nat. Mater.* **2002**, *1*, 91–2.

[29] C. T. Rodgers, *Pure Appl. Chem.* **2009**, *81*, 19–43.

[30] K.-N. Hu, H. Yu, T. M. Swager, R. G. Griffin, *J. Am. Chem. Soc.* **2004**, *126*, 10844–10845.

[31] A. Abragam, M. Goldman, *Reports Prog. Phys.* **1978**, *41*, 395–467.

[32] A. Zagdoun, G. Casano, O. Ouari, M. Schwarzwälder, A. J. Rossini, F. Aussenac, M. Yulikov, G. Jeschke, C. Copéret, A. Lesage, P. Tordo, L. Emsley, *J. Am. Chem. Soc.* **2013**, *135*, 12790–12797.

[33] C. R. Timmel, K. B. Henbest, *Philos. Trans. R. Soc. London, Ser. A Math. Phys. Eng. Sci.* **2004**, *362*, 2573–2589.

[34] K. M. Salikhov, Y. N. Molin, R. A. Sagdeev, A. L. Buchachenko, *Spin Polarization and Magnetic Field Effects in Radical Reaction*, Elsevier, **1984**.

[35] K. Lüders, K. M. Salikhov, *Chem. Phys.* **1987**, *117*, 113–131.

[36] K. Schulten, A. Weller, *Biophys. J.* **1978**, *24*, 295–305.

[37] Y. Sakaguchi, *Mol. Photochem.* **2002**, *46*, 18–21.

[38] U. Werner, Y. Sakaguchi, H. Hayashi, G. Nohya, R. Yoneshima, S. Nakajima, A. Osuka, *J. Phys. Chem.* **1995**, *99*, 13930–13937.

[39] G. Ferraudi, *J. Phys. Chem.* **1993**, *97*, 11929–11936.

[40] W. Schlenker, T. Ulrich, U. E. Steiner, *Chem. Phys. Lett.* **1983**, *103*, 118–123.

[41] A. R. O'Dea, A. F. Curtis, N. J. B. Green, C. R. Timmel, P. J. Hore, *J. Phys. Chem. A* **2005**, *109*, 869–873.

[42] Z. Schulten, K. Schulten, *J. Chem. Phys.* **1977**, *66*, 4616–4634.

[43] D. Canet, C. Aroulanda, P. Mutzenhardt, S. Aime, R. Gobetto, F. Reineri, *Concepts Magn. Reson. Part A* **2006**, *28A*, 321–330.

[44] R. W. Adams, J. a Aguilar, K. D. Atkinson, M. J. Cowley, P. I. P. Elliott, S. B. Duckett, G. G. R. Green, I. G. Khazal, J. López-Serrano, D. C. Williamson, *Science* **2009**, *323*, 1708–1711.

[45] M. C. D. Tayler, M. H. Levitt, *Phys. Chem. Chem. Phys.* **2011**, *13*, 9128–30.

[46] M. Carravetta, M. H. Levitt, *J. Chem. Phys.* **2005**, *122*, 214505.

[47] H. Lee, N. Yang, A. E. Cohen, *Nano Lett.* **2011**, *11*, 5367–72.

[48] Z. Zhang, Y. Xie, X. Xu, H. Pan, R. Tang, *J. Cryst. Growth* **2012**, *343*, 62–67.

[49] S. Knez, C. Pohar, *J. Colloid Interface Sci.* **2005**, *281*, 377–388.

[50] F. Alimi, M. Tlili, M. Ben Amor, C. Gabrielli, G. Maurin, *Desalination* **2007**, *206*, 163–168.

[51] J. S. Baker, S. J. Judd, *Water Res.* **1996**, *30*, 247–260.

[52] K. Kakimoto, M. Eguchi, H. Ozoe, *J. Cryst. Growth* **1997**, *180*, 442–449.

[53] Y. Funasako, T. Mochida, T. Inagaki, T. Sakurai, H. Ohta, K. Furukawa, T. Nakamura, *Chem. Commun. (Camb).* **2011**, *47*, 4475–4482.

[54] M. Mastrangeli, S. Abbasi, C. Varel, C. Van Hoof, J.-P. Celis, K. F. Böhringer, *J. Micromech. Microeng.* **2009**, *19*, 83001–83037.

[55] N. B. Crane, O. Onen, J. Carballo, Q. Ni, R. Guldiken, *Microfluid. Nanofluidics* **2012**, *14*, 383–419.

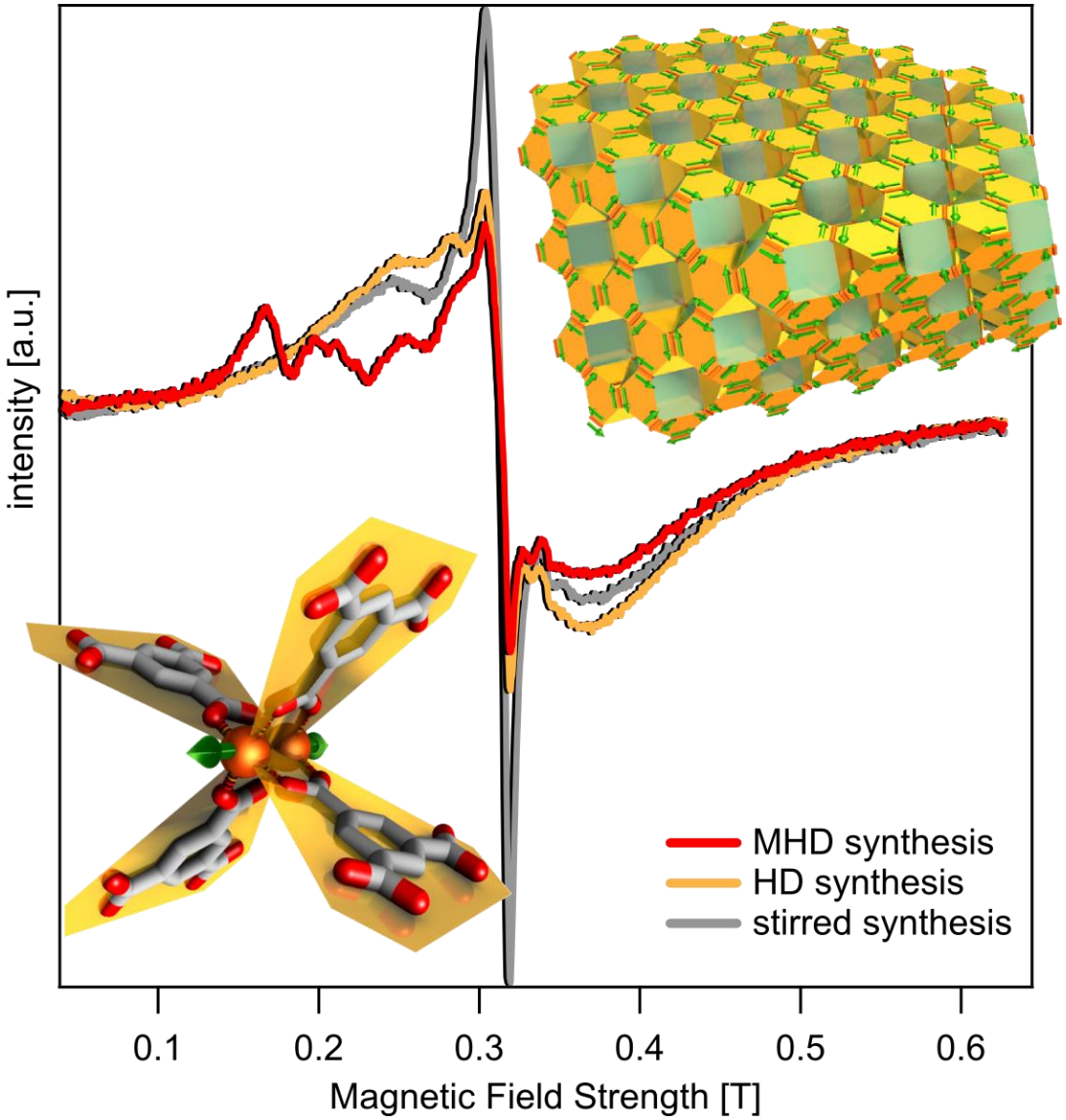

Figure 1: Room temperature EPR spectra of COK-16 for a stirred, hydrodynamic (HD) and magneto-hydrodynamic (MHD) synthesis using a static magnetic field of 0.3 T. Measurements at 140 K are provided in the supplementary material (Figure S1). The inset on the left shows a Cu paddle wheel, the basic building block of the structure. The one on the right provides a general view of the COK-16 structure, where the Cu-pairs are arranged in a Kagomé lattice [28] in the 111 planes. Green arrows illustrate the alignment of the magnetic moments.

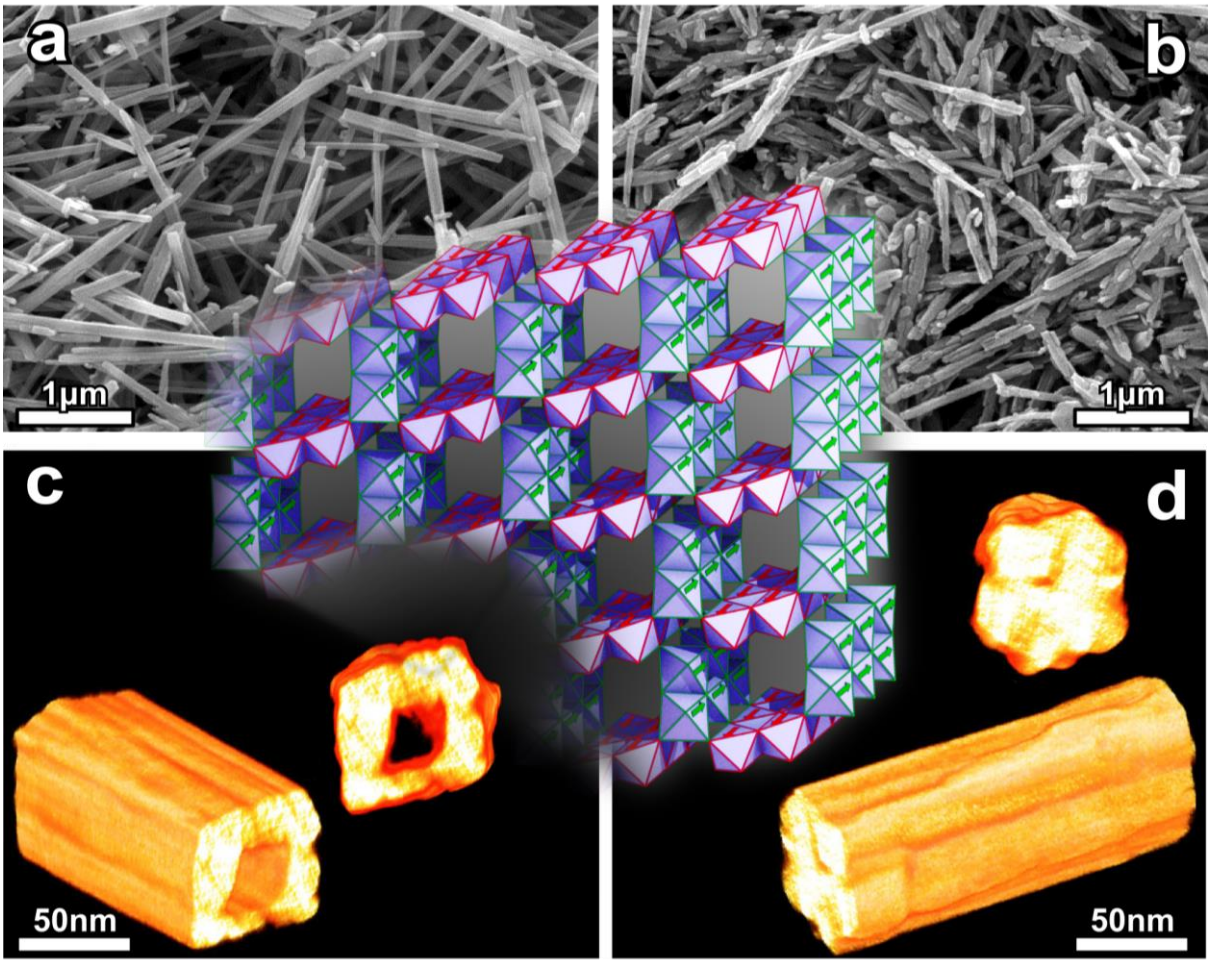

Figure 2: MnO_2 nanotubes after hydrothermal treatment, obtained from reaction mixtures pretreated in presence (a,c) and absence (b,d) of an external magnetic field (B = 0.3 T). a and b: SEM images, c and d: Electron tomography showing the particle morphology along different viewing directions. The inset (center) illustrates the crystal structure of α-MnO_2. The differently colored octahedra symbolise opposite alignment of the magnetic moments.

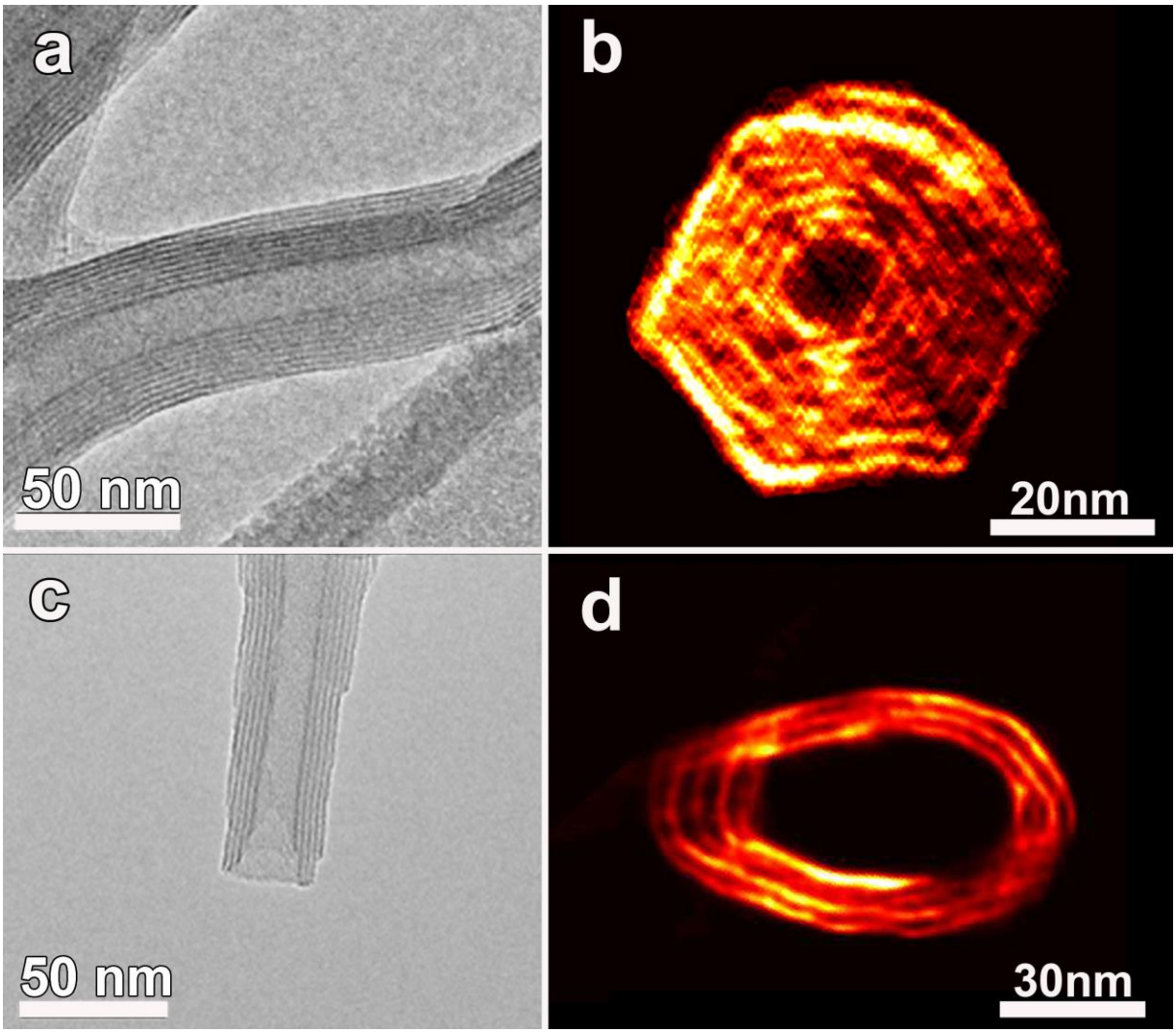

Figure 3: Conventional bright field transmission electron microscopy images of vanadium oxide nanotubes (VOx-NTs) obtained after hydrothermal aging of precursor gels pretreated with MHD and HD are presented in Figure 3 a and c respectively. These images only correspond to 2 dimensional projections of 3 dimensional objects. Therefore, electron tomography was used and cross sectional slices through the (3 dimensional) reconstructed volume are presented in Figure 3 b and d. Note the improved ordering and increased layer stacking in the tube walls, highlighted by a well-defined hexagonal cross-section of the tube compared to a rather tubular, oligo-layered cross-section of the sample derived from HD pretreated gels.

Magnetic Field Assisted Ordering of Electron Spins in Nanoscroll, Nanorod and MOF Formation Processes

Weak external magnetic fields applied on a recirculating synthesis mixture innovates formation of materials containing antiferromagnetically coupled paramagnetic ions. This magneto-hydrodynamic effect is demonstrated for three different, technologically relevant materials: COK-16 metal organic framework, manganese oxide nanotubes and vanadium oxide nano-scrolls.

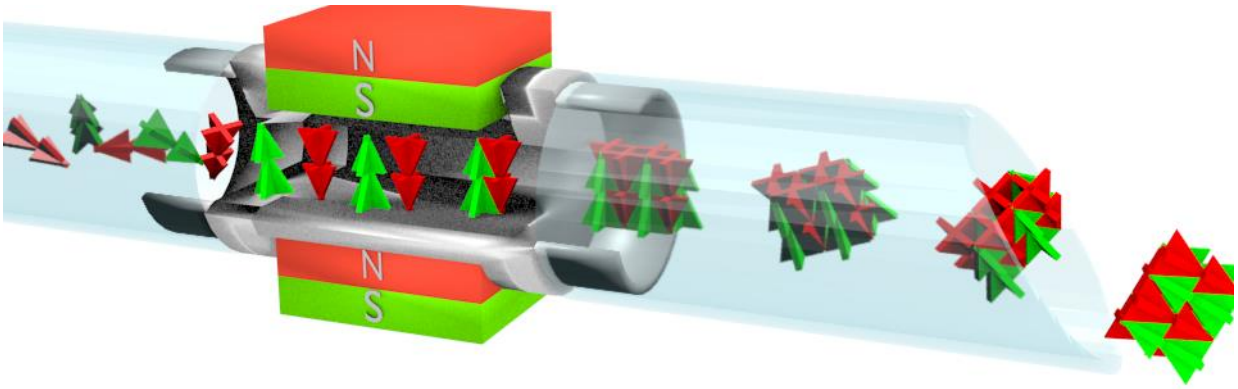

Supporting Information

Magnetic Field Assisted Ordering of Electron Spins in Nanoscroll, Nanorod and MOF Formation Processes

Eric Breynaert[a,*], Jens Emmerich [a], Danilo Mustafa [a,†], Sneha R. Bajpe [a, ‡], Thomas Altantzis[b], Kristof Van Havenbergh[b], Francis Taulelle [a], Sara Bals [b], Gustaaf Van Tendeloo [b], Christine E.A. Kirschhock [a,*], Johan A. Martens [a]

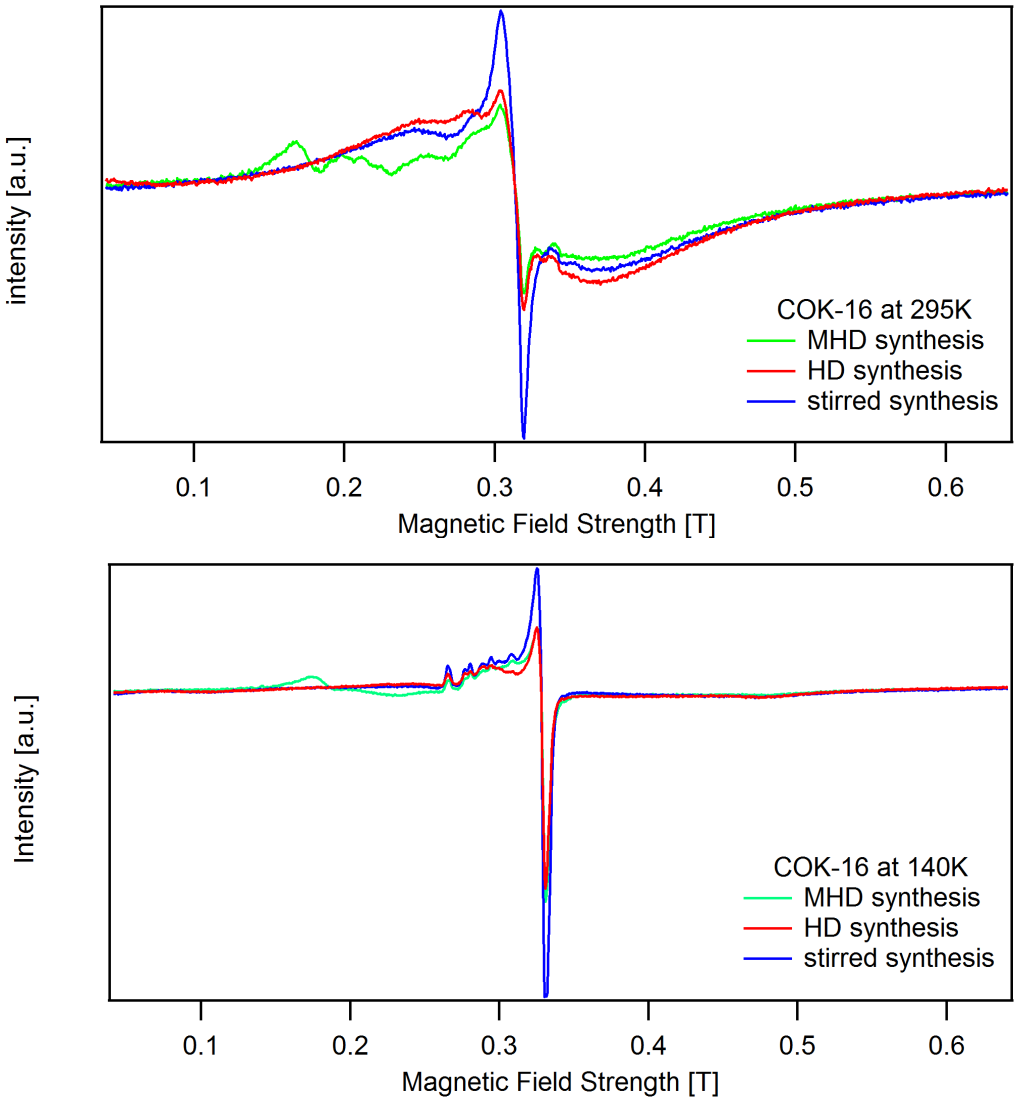

Figure S 1: COK-16 EPR spectra recorded at 295 K (top) and 140 K (bottom) for a stirred, hydrodynamic (HD) and magneto-hydrodynamic (MHD) synthesis using a static magnetic field of 0.3 T. All samples were first recorded at RT followed by data collection at 140 K.

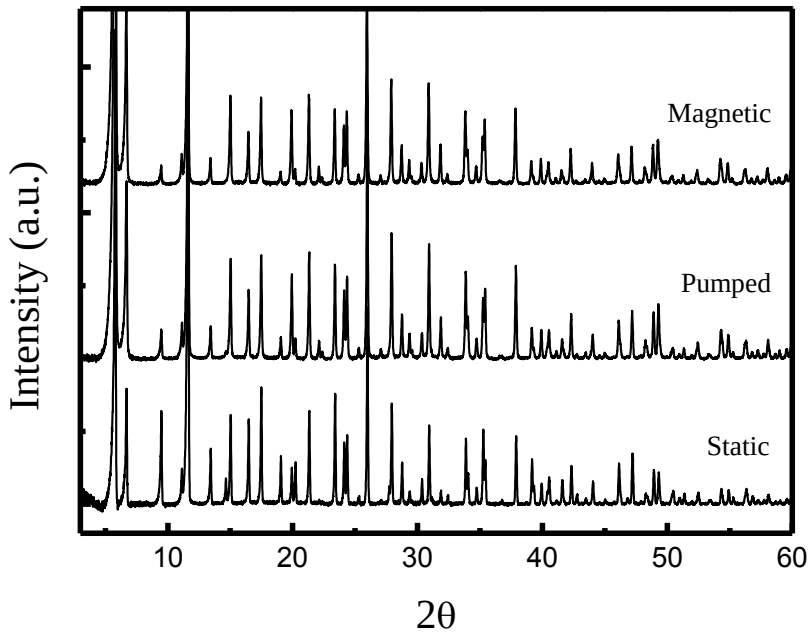

Figure S 2: PXRD patterns for COK-16 samples prepared by mixing the synthesis solutions in a hydrodynamic mixing system in presence and absence of a static magnetic field of 0.3 T applied transverse to the flow.

Figure S 2 shows the PXRD patterns for COK-16mailto:HPA@Cu3(BTC)2.3H2O samples prepared from the same starting solution but aged at in a hydrodynamic mixing systems respectively in presence and absence of a 0.3 T external magnetic field applied transverse to the flow. Refinement of this series of identical patterns resulted in similar unit cell parameters (spacegroup *Fm3m*, unitcell dimensions respectively 26.3169 and 26.3280Å).

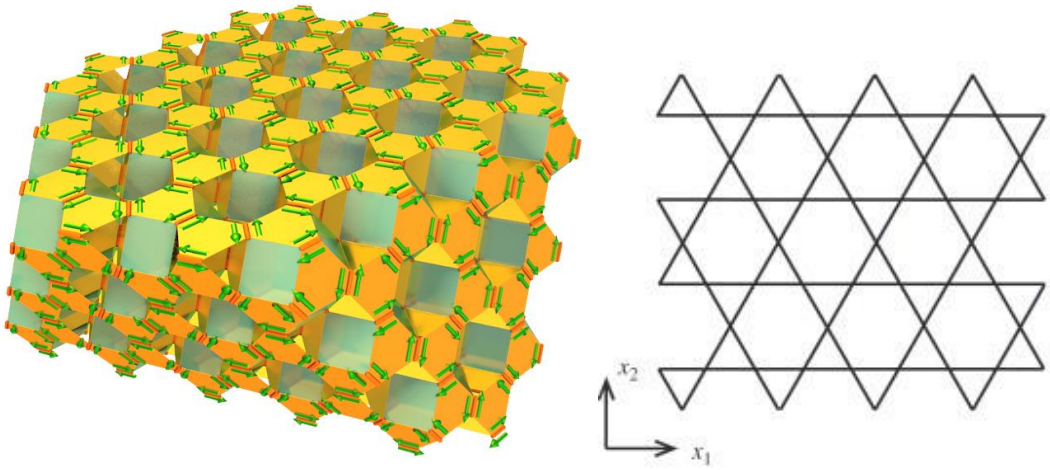

Figure S 3: COK-16 structure (left) showing the Kagomé lattice (right) found in the 111 planes. Superexchange coupled Cu^{2+} ions are located on each corner of the triangles.

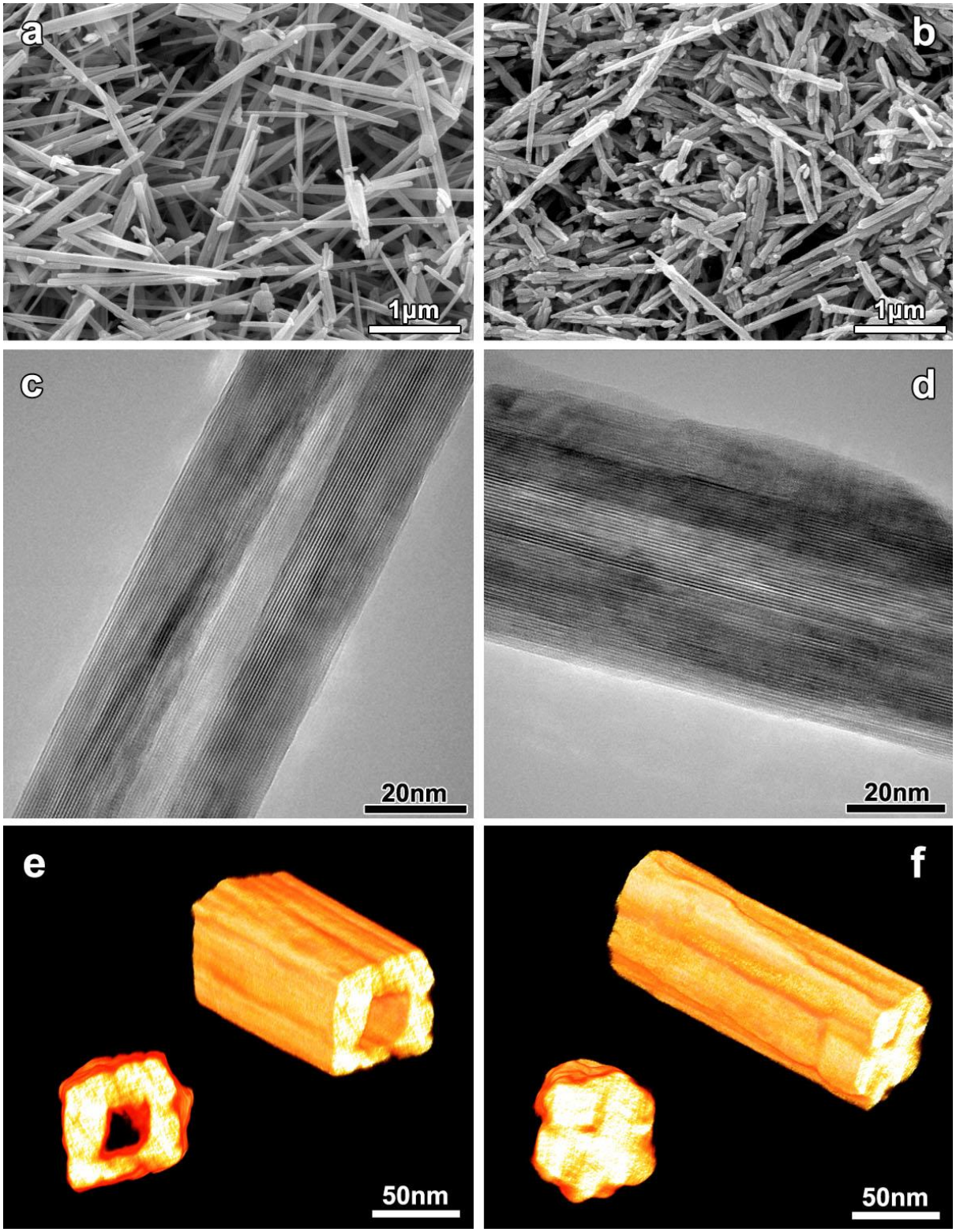

Figure S 4: MnO_2 nanotubes after hydrothermal treatment, obtained from reaction mixtures pretreated in presence (a,c,e) and absence (b,d,f) of an external magnetic field (B = 0.3 T). a and b: SEM images of MnO_2 nanotubes pretrated in presence and absence of an external magnetic field respectively, c and d: High Resolution TEM images of MnO_2 nanotubes pretrated in presence and absence of an external magnetic field respectively. The EM images only correspond to 2 dimensional projections of 3 dimensional objects. Therefore, electron tomography was used and 3D visualizations of the nanotubes is presented along different viewing directions.

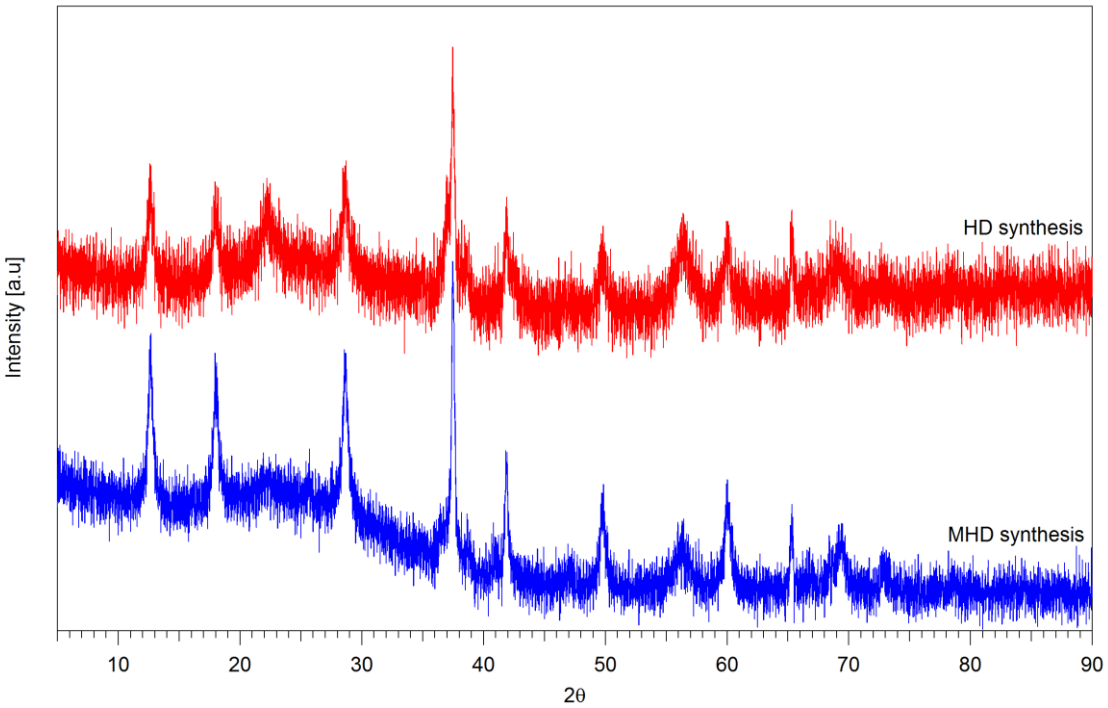

Figure S 5: PXRD patterns for MnO_2 nanotubes after hydrothermal treatment, obtained from reaction mixtures pretreated in presence (MHD) and absence (HD) of an external magnetic field (B = 0.3 T).